Biochimica et Biophysica Acta 1853 (2015) 2984–2991

Contents lists available at ScienceDirect

Biochimica et Biophysica Acta

journal homepage: www.elsevier.com/locate/bbamcr

Crowding of receptors induces ring-like adhesions in model membranes☆

Daniel Schmidt [a,b], Timo Bihr [a,b], Susanne Fenz [c,d], Rudolf Merkel [c], Udo Seifert [b], Kheya Sengupta [e], Ana-Sunčana Smith [a,f,*]

[a] Institut für Theoretische Physik and Cluster of Excellence: Engineering of Advanced Materials, Friedrich Alexander Universität Erlangen–Nürnberg, 91052 Erlangen, Germany
[b] II. Institut für Theoretische Physik, Universität Stuttgart, 70569 Stuttgart, Germany
[c] Institute of Complex Systems 7: Biomechanics, Forschungszentrum Jülich GmbH, 52425 Jülich, Germany
[d] Lehrstuhl für Zell- und Entwicklungsbiologie (Zoologie I), Biozentrum der Universität Würzburg, 97074 Würzburg, Germany
[e] Aix-Marseille Université, CNRS, CINaM UMR 7325, 13288 Marseille, France
[f] Insitut Ruđer Bošković, 10000 Zagreb, Croatia

ARTICLE INFO

Article history:
Received 9 March 2015
Received in revised form 21 May 2015
Accepted 22 May 2015
Available online 28 May 2015

Keywords:
Cell adhesion
Immunological synapse
Adhesion dynamics
Membrane transmitted correlations
Ligand-receptor bonds
Crowding effects
Membrane fluctuations
Diffusion–reaction systems

ABSTRACT

The dynamics of formation of macromolecular structures in adherent membranes is a key to a number of cellular processes. However, the interplay between protein reaction kinetics, diffusion and the morphology of the growing domains, governed by membrane mediated interactions, is still poorly understood. Here we show, experimentally and in simulations, that a rich phase diagram emerges from the competition between binding, cooperativity, molecular crowding and membrane spreading. In the cellular context, the spontaneously-occurring organization of adhesion domains in ring-like morphologies is particularly interesting. These are stabilized by the crowding of bulky proteins, and the membrane-transmitted correlations between bonds. Depending on the density of the receptors, this phase may be circumvented, and instead, the adhesions may grow homogeneously in the contact zone between two membranes. If the development of adhesion occurs simultaneously with membrane spreading, much higher accumulation of binders can be achieved depending on the velocity of spreading. The mechanisms identified here, in the context of our mimetic model, may shed light on the structuring of adhesions in the contact zones between two living cells. This article is part of a Special Issue entitled: Mechanobiology.

1. Introduction

Reorganization of cell surface molecules at the adhesive interface is recognized as an essential feature of cell adhesion and has been extensively studied in the context of integrins, cadherins, and many other cell adhesion molecules [1–6]. A particularly intriguing example is the drastic molecular rearrangement at the interface between a T lymphocyte and an antigen presenting cell, leading to the formation of concentric rings, each enriched in certain specific cell surface molecules [1]. Interestingly, T cells interacting with supported lipid bilayers (SLBs) carrying mobile ligands reproduce this phenomenon [2], and studies on such hybrid systems have revealed the detailed structure and dynamics of formation of these so called SMACs (Supra Molecular Adhesion Structures) [4,3] and elucidated the connection to receptor mobility [5]. From a theoretical perspective, several groups have proposed different effects as the possible driving mechanism for ring-like SMAC formation. These include differences in binding affinity and stiffness [7,8], biased diffusion of antigen complexes towards the interior of the synapse [9] and membrane driven interaction between binding pairs of different lengths [10–15]. The current consensus in the immunology community, based on seemingly decisive experiments with size modified binders [16,17], is that if two types of binders are not of different length the segregation is disrupted. In this context, theoretical considerations suggest that even with two binders, ring-like SMACs are unstable [12].

However, recent experiments showed that the T cell receptor is actually driven by actin, obviating the need to invoke the difference in length between the receptors to explain segregation [4].

Very recently, a ring like structure was also found during the formation of tight junctions in spreading epithelial cells [6]. While the late stage of spreading, which takes place after the ring is formed, is clearly driven by actin, the mechanism for the initial structuring of cadherin adhesions into a ring like structure is not yet understood [6].

Adhesion experiments with model membranes, where the cell in hybrid systems described above is replaced by a giant unilamellar vesicle (GUV, for a sketch of the model see Fig. 1), have furthered our understanding of membrane adhesion, and have vastly aided theoretical

☆ This article is part of a Special Issue entitled: Mechanobiology.

* Corresponding author at: Institut für Theoretische Physik and Cluster of Excellence: Engineering of Advanced Materials, Friedrich Alexander Universität Erlangen–Nürnberg, 91052 Erlangen, Germany and Insitut Ruđer Bošković, 10000 Zagreb, Croatia.
E-mail address: smith@physik.uni-erlangen.de (A.-S. Smith).

http://dx.doi.org/10.1016/j.bbamcr.2015.05.025
0167-4889/

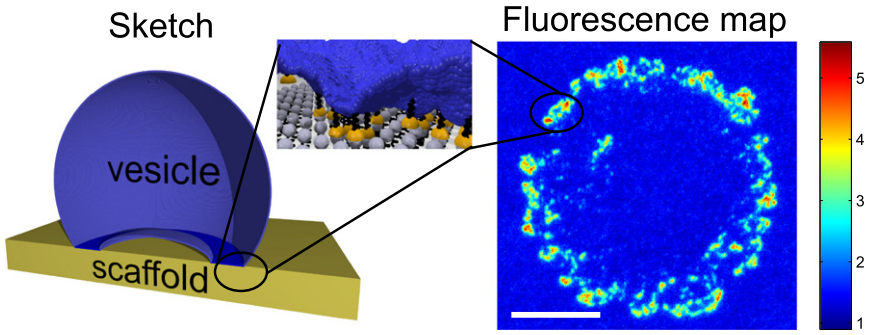

Fig. 1. Left: Cartoon of the system involving a vesicle (blue) which adheres to a scaffold (yellow). The specific adhesion domain (dark-blue and zoom-in on right side) forms a ring. For better visibility, a cut through the vesicle is shown. The inset visualizes a typical microscopic membrane profile. Vertical and lateral dimensions are not to scale. Right: Fluorescence map of a vesicle showing the accumulated receptors in a color code (units in 10^3 μm^{-2}). The scale bar is 10 μm.

modeling [18–20]. In many cases, especially if the GUV is floppy, a ring like domain was seen [21]. However, in most of these cases, the ring, observed in reflection interference contrast microscopy (RICM) images as a dark domain, is transient [21]. One notable exception was reported recently where biotin carrying GUVs adhering to neutravidin carrying SLBs gave rise to SMAC like rings of fluorescent labeled receptors [22]. These rings, formed under conditions of receptor shortage, were reported to be long lived and seemingly stable.

From a theoretical point of view, a thermodynamically stable ring-like domain should be associated with a global minimum of the free energy of adhesion. The latter can be calculated for a fixed number of bonds confined to a particular configuration (see Fig. 2). In this case, the free energy of an adhesion domain emerges as a sum over all bonds for the gain in binding enthalpy and the cost for deforming both the flexible membrane and the adhesion proteins. Additional entropic costs emerge from confining the diffusive binders upon the formation of the bond [23–25] and for suppressing membrane fluctuations. Such a free energy possesses a global minimum for a topologically circular domain where the bond density is not maximal, but is determined by balance of energetic terms that favor maximal bond density and the entropic terms that push the bonds apart. However, we find that in addition to the global minimum, a local minimum exists for a ring-like topology. Since the free energy difference between the global and the meta-stable ring configuration is of several k_BT per bond (see Fig. 2), it is not clear, even for model membranes, what leads to the formation of adhesions in a ring configuration. In the cellular context, coupling to the actin was found to play a major role at longer time scales, but the mechanism for the selective binding at the edge of the contact zone has not been clearly identified yet.

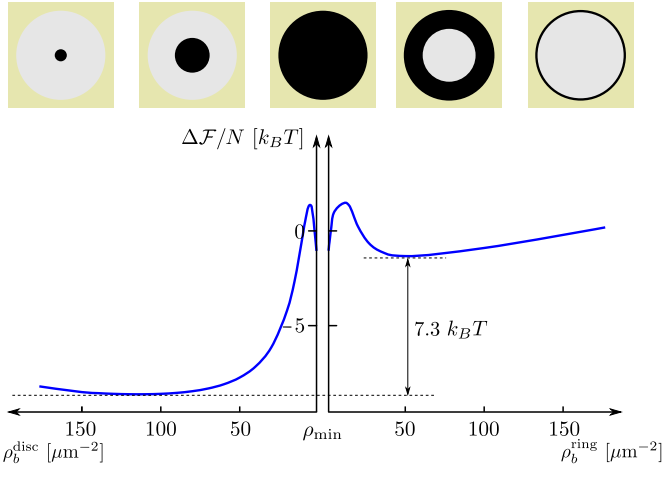

Fig. 2. Free energy per bond $\Delta\mathcal{F}/N$ for a bond domain with a circular (left) and ring like (right) shape. The sketches in the top row illustrate the domain area (black) in the contact zone (gray) accordingly to the axis in the graph. For the circular domain the bond density decreases from left to right while for the ring-like domain it increases. The number of bonds is fixed to $N_b = 200$ for all bond densities with $\rho_{\min} \approx 1.4$ μm^{-2}. All other parameters are chosen according to Table 1.

The aim of our current work is to deepen the understanding of the physical mechanisms that determine the number of adhesion domains, their growth patterns and final morphology. The goal is to identify physical mechanisms that drive the formation of ring-like adhesions, which were experimentally observed in model systems but also in the cellular context. In the latter case, this work may shed light on the role of active processes (not considered here explicitly), which can be used to control the dynamics and the emergent structure of adhesions, including the ring-shaped domains. We achieve this goal by performing an extensive theoretical analysis of the experimentally observed phenomena. We show that ring like structures appear spontaneously in vesicular systems due to the interplay of slow protein diffusion and fast binding kinetics, which results in the formation of bonds at the periphery of the vesicle-substrate contact zone. Furthermore, we find that the necessary conditions for the formation of stabilized rings are (i) the mobility of both binding partners, (ii) membrane transmitted correlations, (iii) bulkiness of binders which allows for crowding and (iv) a significant slowing down of bulky receptors upon binding.

Following this introduction, we first present details of the experimental and simulation procedures. We proceed with constructing the phase diagrams of adhesion for mobile and immobile receptors on the supported bilayer. We analyze and analytically model the identified regimes of growth, and study the stability of ring-like structures. We compare our theoretical framework to the experimental result, and find excellent agreement between the two approaches.

2. Experimental methods

Giant unilamellar vesicles (GUVs) containing a specified amount (0.1 to 5%) of DOPE-cap-biotin (1,2-dioleoyl-sn-glycero-3-phosphoethanolamine-N-(cap biotinyl)) and 2% DOPE-PEG2000 (1,2-dioleoyl-sn-glycero-3-phosphoethanolamine-N-(methoxy (polyethyleneglycol)-2000)), dispersed in a matrix of SOPC (1-stearoyl-2-oleoyl-sn-glycero-3-phosphocholine) (all from Avanti Polar Lipids, Alabaster), are prepared by electro-swelling [26]. Supported lipid bilayers (SLBs) of equivalent composition are prepared by the Langmuir–Blodgett/Langmuir–Schäfer technique and are functionalized with neutravidin covalently linked to the fluorescent label Oregon Green or tetra-methylrhodamine (neutravidin-fl, both Invitrogen, Eugene, OR) and suitable passivated with bovine serum albumin (BSA, 98% purity, Sigma, Saint Louis, MO) (both reconstituted in PBS buffer and ultracentrifugated to eliminate protein aggregates) [26]. The experimental design ensures that both ligands (biotins) and receptors (neutravidins) are mobile [26]. The amount of biotinylated lipids in the GUV and SLB determines the density of ligands and receptors,

respectively. In a typical experiment, 10 μl of the vesicle solution is added to the SLB in a total volume of 1 ml PBS buffer.

Vesicles adhering in steady state are identified by imaging with reflection interference contrast microscopy (RICM) [27,28]. The corresponding receptor distribution of neutravidin-fl is recorded with epifluorescence microscopy using a 63× Antiflex Plan-Neofluar 1.25 oil objective.

The enrichment factor of the receptors, which reflects how much receptors are accumulated in the contact zone, relative to the bulk density, is calculated as described earlier [22]. The diameters of GUVs are determined from phase contrast microscopy in the final state and typically range from 20 to 30 μm.

3. Simulation method

To simulate the process of domain formation we use our recently developed Monte Carlo approach [29]. In this scheme, the vesicle membranes and the SLB membranes are represented by rectangular superimposed grids (lateral size of 40.96 μm), functionalized with ligands and receptors, respectively. To account for different sizes of ligands and receptors, the two lattices have different lattice constants (the lattice constant of the ligand grid is 8 times smaller (4096×4096 lattice nodes) than that of the receptor grid).

A circular region is selected on each membrane to represent a contact zone. Both the vesicle membrane and the SLB are treated as reservoirs with a constant number of binders. In both cases periodic boundary conditions for binder diffusion are imposed at the edge of the system. Diffusion is simulated by a simple random walk (diffusion constant D) of particles that mutually interact in the plane of the membrane by hard core repulsion.

To simulate creation and disruption of bonds, we use effective binding and unbinding rates [30], which are sensitive to the local configuration of bonds [31], and integrate the local shape and fluctuations of the vesicle membrane [29]. Binding attempts take place when a free ligand and a free receptor find each other at the same lateral position. Motivated by experimental findings [32,26] which suggest a drastic decline of the mobility of a ligand-receptor complex compared to the diffusion of the unbound species, the formation of a bond is associated with the immobilization of the involved ligand and receptor. If a bond breaks, the ligand and the receptor regain their initial mobility.

The simulation starts by randomly placing ligands on their lattice (lattice constant a) such that the desired ligand density ρ_l^0 is obtained. Furthermore, if the receptors are deemed immobile, they are regularly spaced on their lattice at separations of $\bar{r} = 1/\sqrt{\rho_r^0}$. Alternatively, when simulating mobile receptors, a randomly distributed starting configuration is generated, with the appropriate density ρ_r^0. The simulation is executed until the number of bonds saturates for a significant amount of time.

To be able to compare with experiments, in the simulation we choose the membrane bending rigidity to be $\kappa = 20\ k_BT$ [33], the strength of the interaction potential $\gamma = 6.5\ \mathrm{J/cm^2}$ [34]. The difference between the equilibrium position of the unbound vesicle membrane and the height for specific adhesion to the substrate is set to $\Delta h = 45$ nm and the vesicle radius is $R = 11.6$ μm with a volume fraction of 97.5% (standard average conditions in the experiments). The binding enthalpy of the biotin–neutravidin bond is taken to be $\epsilon_b \approx 10\ k_BT$ in accordance with previous estimates [22] for the enthalpy of membrane bound biotin–neutravidin bonds, which is considerably weakened because of the coupling of the ligands and receptors to the membrane. All parameters are summed up in Table 1.

Table 1
Parameters used in the simulations.

	Meaning	Value
a	Lattice constant	10 nm
k_BT	Thermal energy at 300 K	$4.14 \cdot 10^{-21}$ J
κ	bending rigidity [33]	20 k_BT
γ	Curvature of the interac. pot.†	6.5 J/cm^4
Δh	Distance between equilibrium Positions of membr. and bond†	45 nm
λ	Stiffness of the bond/receptor*	0.21 mJ/m^2
ϵ_b	Binding enthalpy [22]	9.55 k_BT
D	Diffusion constant [26]	5.0 μm^2/s
R_c	Radius of contact zone†	6.81 μm
d	Lateral size of simulation box (size of the vesicle)†	40.96 μm

† Measured.
* Typical value from literature.

4. Morphological phase diagram

The analysis of simulation and experimental data shows that there are, in principle, four regimes of adhesion processes, mainly determined by the initial ligand and receptor density (Fig. 3). The first is the regime of unstable adhesion at low ligand and receptor densities. Increasing the density of at least one of the binders enables adhesion. Several morphologically different processes ensue. If the density of ligands is larger than the receptor density, numerous randomly distributed nucleation seeds form within the contact zone. The domains grow independently of each other until they come in direct contact and merge, developing further as a large, single domain. We denote this as the regime of multiple nucleation (first row in Fig. 3C). At higher densities of immobile receptors we find a transient ring regime (second row in Fig. 3C). It occurs because ligands diffuse from the bulk of the vesicle into the contact zone, where they bind to the surplus of receptors close to the edge of the contact zone, forming a ring. However, due to the small size of ligands, they are able to diffuse through a bond domain restoring the ligand density in the interior of the ring and continue thickening the ring. Furthermore, upon unbinding from the inner edge of the ring, the ligands move deeper into the contact zone, making the ring morphology only transient. At low densities of mobile receptors, the ring morphology is stabilized by the inability of bulky receptors to penetrate the contact zone (stable ring shown in the third row in Fig. 3C). The large packing density of receptors stabilizes the morphology on time scales that are significantly longer than those accessible in an experiment (stable ring regime).

4.1. Unstable adhesion

For very small ligand and receptor densities, only single bonds opening and closing over the whole contact zone could be observed without ever forming a stable nucleus. We also find that for the current choice of the binding affinity, temperature and membrane bending stiffness, enthalpic arguments [30] predict the critical size of the seed to be two or more bonds. Actually, for immobile receptors, the critical size of the nucleus diverges if the density of bonds (receptors) or ligands becomes too low (dashed line in Fig. 3). For mobile ligands, the density of bonds is self-regulated and typically sufficiently large, such that the adhesion should never be impeded. Indeed, the unstable regime occurs at significantly lower densities than for immobile receptors. However, eventually the domains no longer appear even if receptors are mobile, which suggests that the nucleation process is diffusion limited at very low binder densities. Namely, while the ligands and receptors form occasionally one bond, the time necessary for another pair of binders to diffuse and form the second bond is longer than the life time of the first bond. This, in effect, impedes nucleation.

4.2. Multiple nucleation

This growth regime is reaction limited (initial receptor density ρ_r^0 smaller than initial ligand density ρ_l^0) and it occurs because the nucleation rate is large (the full lines indicate the cross-over from diffusion to reaction limited regimes in Fig. 3A and B). However, the multiple

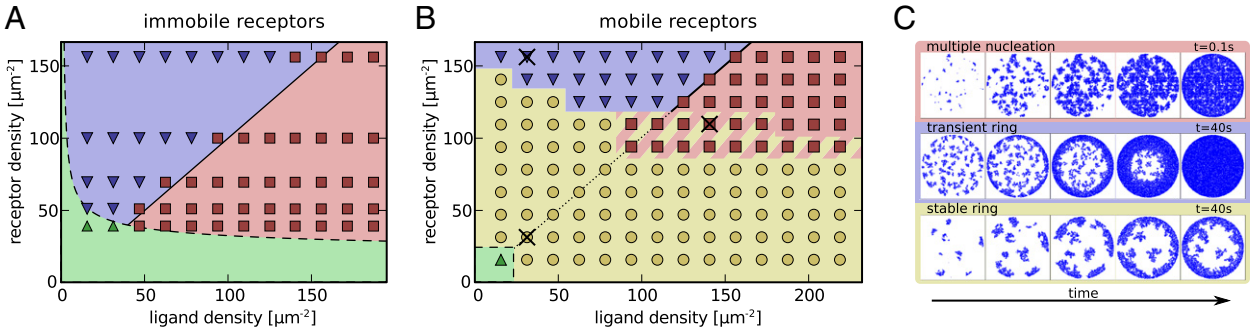

Fig. 3. Phase diagrams for immobile (A) and mobile receptors (B), showing the four regimes of growth: (i) unstable adhesion (green) (ii) regime of multiple nucleation (red) characterized by the formation of small domains all over the contact zone, (iii) transient rings (blue), (iv) stable rings (yellow). (C) Time evolution of adhesions in the contact zone for the three adhesive regimes. The particular parameters are marked in (B) with crosses. Growth dynamics of adhesion obtained in simulations is provided in supplementary material in a form of a movie for each phase.

nucleation regimes are not always accessible in the phase space. For example, a smaller binding affinity leads to a coarsening of the adhesion process, i. e. larger individual adhesion domains and fewer nucleation seeds, and ultimately to radial growth [35]. While having immobile receptors, we find this regime to overlap with the reaction limited part of the phase space, for mobile receptors multiple nucleation occurs at high binder densities where diffusion into the contact zone plays no role and the receptors are almost immobile due to crowding. On the other hand, the surplus of ligands keeps the nucleation rate constant.

This situation is well accounted by the Johnson–Mehl−Avrami–Kolmogorov-theory (JMAK) [36,37] describing the growth dynamics of domains that nucleate at constant nucleation rate Γ and grow with a radial velocity v, independent of time. Under these conditions the number of bonds as a function of time is given by [37]

$$N_b(t) = N_{\mathrm{eq}}\left(1-\exp\left[-\frac{\pi}{3}\Gamma v^2 t^3\right]\right) \tag{1}$$

where N_{eq} denotes the number of bonds in equilibrium and the growth curve has a cubic time dependence in the exponent.

A comparison of this theory with exemplary simulation data with mobile (Fig. 4, yellow diamonds) and immobile receptors (red squares and blue circles) shows reasonable agreement. Small deviations in the growth law arise because the domains do not grow independently due to the relatively small area they are confined to. Furthermore, the vesicle reservoir of ligands becomes depleted over time, affecting both the nucleation rate and the growth velocity. Ultimately, the simulation growth curve saturates and the equilibrium state is achieved.

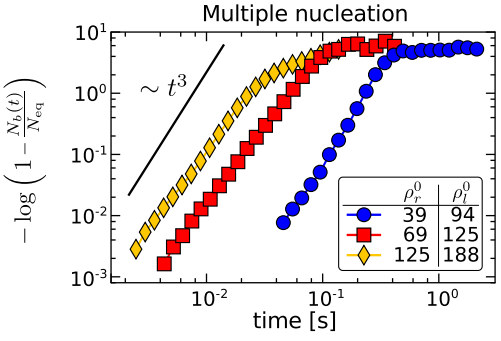

Fig. 4. Avrami plot for three exemplary curves of domain growth in the multiple nucleation regime. The solid black line is a cubic function for comparison with analytical prediction, Eq. (1). Yellow diamonds originate from mobile receptors whereas red squares and blue circles belong to immobile receptors. The densities in the legend are in units of μm^{-2}.

4.3. Transient ring

The formation of a transient ring morphology (blue shaded regions in Fig. 3 A and B) is driven by the diffusion of ligands into the contact zone, where an enthalpy gain is induced upon binding. The formation of transient rings occurs if the initial density of receptors is larger than the initial density of ligands, and if the diffusion of receptors plays no role (immobile receptors or high density of mobile receptors). Because of the relatively large binding affinity, and the surplus of receptors, the ligands bind relatively fast after penetrating the contact zone. This promotes nucleation and a faster growth of domains at the periphery of the contact zone. Eventually, these domains merge and form a ring (identified as an enhancement in the radially averaged bond density close to the edge of the contact zone, relative to the density at the center). However, because of their small size, ligands can move between bonds in the ring. If not bound in the ring, the ligands may penetrate through the ring and bind to free receptors in the interior of the contact zone. This leads to thickening of the ring until it is completely transformed to a disk and the entire contact zone is filled with bonds (second row in Fig. 3C).

As the limiting time scale of the ring closure is determined by diffusion dynamics, the reaction kinetics, earlier important in the regime of multiple nucleation, do not need to be considered. Hence, the dynamics ensuing the establishment of the ring can be modeled by the radially symmetric diffusion equation for the ligand density $\rho_l(r,t)$ [38–41]

$$\frac{\partial \rho_l(r,t)}{\partial t} = D\left(\frac{\partial^2 \rho_l(r,t)}{\partial r^2} + \frac{1}{r}\frac{\partial \rho_l(r,t)}{\partial r}\right). \tag{2}$$

Here D is the diffusion constant of ligands, the radial distance r is measured from the center of the contact zone, and the bond density within the ring will be denoted by ρ_b. This equation is accompanied with a moving boundary condition for the inner radius $R(t)$ of the ring

$$\frac{\partial R(t)}{\partial t} = -\frac{D}{\rho_b}\frac{\partial \rho_l(r,t)}{\partial r}\bigg|_{r=R(t)}, \tag{3}$$

and the density of ligands at the inner interface

$$\rho_l(R(t),t) = \rho_l^e. \tag{4}$$

Initial conditions intuitively set the density of ligands and the thickness of the ring at $t = 0$ to be

$$\rho_l(r,0) = \rho_l^0, \quad \text{and} \quad R(0) = R_c. \tag{5}$$

Since no full analytic solution is available for this moving boundary problem, Eqs. (2) to (5) are solved numerically for $\rho_l^e = 0$ and ρ_b is extracted from simulations. The solution is compared with the results of

the simulation in Fig. 5A. Without any fit parameters, we find excellent agreement between the two approaches confirming that the closure of the ring is mainly driven by the diffusion of ligands from the bulk of the vesicle into the contact zone.

Interestingly, the dynamics of the ring closure is stable with respect to the shape of the inner interface. This is unusual behavior for diffusion limited growth processes where typically dendritic or even fractal patterns evolve in time [42,43]. However, this can be understood from the ligand density profile around a ring domain with shape perturbations at the inner interface (Fig. 5B). Because the flux of ligands from the outside is larger at trailing parts of the interface than at the leading parts, the shape instability is suppressed and the inner shape of the ring is stabilized.

4.4. Stable rings

Formation of the stable ring morphology (yellow shaded regions in Fig. 3B) is driven by the diffusion of receptors into the contact zone. It occurs at densities where the receptor mobility is not significantly impeded by crowding effects (low receptor densities), but is sufficiently large for stable nucleation to take place. For this reason, the stable ring regime strongly relies on the membrane-transmitted cooperative effects between bonds.

The importance of cooperativity is clearly demonstrated in Fig. 6A, where we show snapshots from a simulation without (left) and with (right) the membrane implicitly resolved. In the first case the formation of bonds does not affect the shape and the fluctuations of the membrane (no cooperativity), hence, the ligand-receptor reaction rates are constant. In the second case, the reaction rate is coupled to the membrane as discussed in the method section. Due to this cooperativity, the bonds organize into domains, and the number of bonds is an order of magnitude larger compared to the case without the membrane transmitted interactions between bonds. In the latter case, the bonds are randomly distributed over the contact zone. In fact, without correlations, nucleation is suppressed, and stable adhesion may not take place. If this occurs, the formation of the ring is significantly delayed. Yet, in the latter case, the closing of the ring occurs on significantly shorter time scales than for stable rings, suggesting a transient ring regime.

The stability of the ring is hence promoted by the cooperative effects which promote binding in the vicinity of already existing bonds. However, because of their size, bulky bound receptors become obstacles for diffusing receptors, which slow down their transport toward the center of the contact zone, and further promote their binding at the edge. This induces crowding of receptors and seals the interior of the contact zone from the outer reservoir of binders. Another consequence of cooperativity is the significantly diminished unbinding rate. Hence, even receptors at the inner edge unbind extremely rarely, which suppresses further thickening of the ring on experimentally accessible time scales.

In very long simulations (Fig. 6B), however, we observe the increase of the ring thickness of about 50% after extending the simulation to an order of magnitude longer than time necessary for the formation of the ring. This suggest, that ultimately, even "stable" ring-like domains are, in essence, transient even though not on accessible time scales. However, as the ring growth depends solely on the unbinding and rebinding of bonds at the inner edge of the ring domain, increasing the effective binding affinity drastically decreases the growth of the ring.

Last but not least, the stability of the phase diagram depends on the system size. For example, decreasing the number of available ligands by keeping the same concentration but decreasing the size of the vesicles, at some point induces a shortage of ligands. Hence, the small domains may not merge to cover the entire contact zone or to close the rings. On the other hand, quadrupling the area of the vesicle (ligand reservoir of 8192×8192 lattice points for a vesicle of a radius $R = 23.1$ μm) induced no changes in the phase diagram.

Additional effects arise from the finite size of the contact zone. It does not affect the regimes of transient ring formation and multiple nucleation. However, for smaller radii of the contact zone, the phase space for the formation of stable rings shrinks because the ring thickness depends only on the concentrations of binders and not on their absolute number. The thickness of the ring is related to the length of the mean free path of a receptor coming from the bulk into the contact zone before forming a bond. If the contact zone is smaller than this mean free path, the receptor can explore the surface entirely, and the contact zone will be filled up with bonds. Conversely, increasing the size of the contact zone increases the phase space associated with stable rings.

5. Comparison with the experiments

5.1. Steady state morphology and size of adhesions

To study the interplay between protein diffusion, binding kinetics, and membrane transmitted correlations in an experimental system, we construct the experimental phase diagram for adhesion of a biotin decorated vesicle that binds to SLB with mobile neutravidins. We systematically change the concentration of neutravidin and of biotin and image the distribution of neutravidin in the steady state in 44 vesicles (Fig. 7A).

In previous work [28], we showed that within biotin–neutravidin adhesions the membrane is nearly flat, very close to the SLB, and fluctuations are completely suppressed (< 1 nm). This suggests that the affinity for biotin–neutravidin binding is very high, and that each neutravidin in the contact zone is bound to its ligand [25]. This is confirmed by simulations where we find that the number of bonds is at least 95% of the number of available receptors, even though the binding affinity used in simulations is smaller than the binding affinity of a biotin–neutravidin

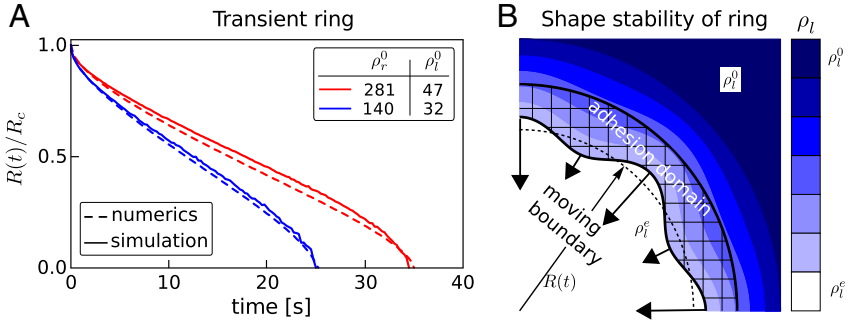

Fig. 5. A) Dynamics of the ring closure from simulations (solid lines) and the numerical model (dashed lines). B) Ligand density profile around a perturbed inner edge of the ring-like domain (shaded with squares). Arrows represent the magnitude and the directions of the flux of ligands towards the interior. The unperturbed interior edge is shown with a dotted line.

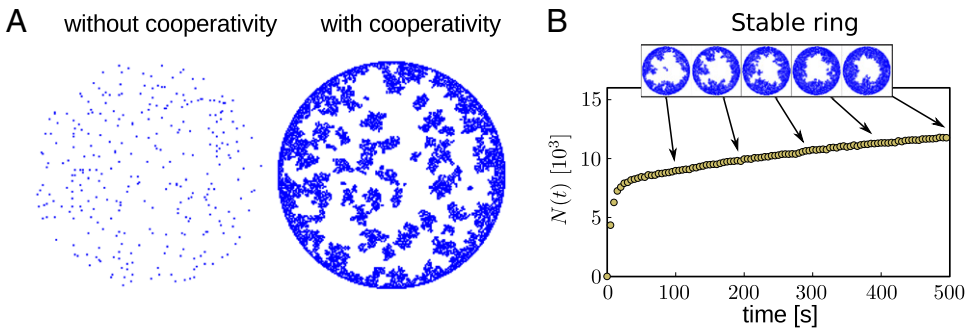

Fig. 6. A) Snapshots of the contact zone in steady state. A snapshot of the contact zone for a system without cooperativity (left), is compared to the contact zone from the full simulation including membrane induced cooperative effects between bonds (right). Both simulations are performed with identical parameters as stated in the simulation method section, except for the effective binding affinity which was increased to 15 k_BT. The binder densities are set to $\rho_l^0 = \rho_r^0 = 31\ \mu m^{-2}$. B) A very long simulation in the stable ring regime with an effective binding affinity of 10 k_BT shows slow thickening of the ring. Increasing the binding affinity slows down the thickening of the ring (data not shown).

pair within adhesions. The same result can be visualized by comparison of the bond and receptor distributions (Fig. 7B and C).

Compared to biotin ligands, neutravidin receptors are very large, and are expected to crowd when penetrating the contact zone, and hence, induce stable rings. Indeed, as in simulations, at high concentrations of receptors the contact zone is uniformly filled with bonds, but decreasing the receptor concentration results in the appearance of ring-like adhesions.

If the concentration of receptors is low, increasing the ligand density for a fixed receptor density, decreases the average area of adhesions (Fig. 7B, bottom rows) and, moreover, the ring thickness d decreases, too (Fig. 8A). For example, for vesicles shown in Fig. 7A, increasing the ligand density by factor of 10 from $\rho_l^0 = 1.4 \cdot 10^3\ \mu m^{-2}$, induces a decrease of the adhesion area from 51% to 35% of the contact zone, and the ring thickness from 3.6 to 2.4 μm (Fig. 8A inset). On the other hand, increasing the receptor density from $\rho_b^0 = 1.4 \cdot 10^3$ to $3.5 \cdot 10^3\ \mu m^{-2}$ for a constant ligand density of $\rho_l^0 = 14 \cdot 10^3\ \mu m^{-2}$, results in the increase of the adhesion area from 35% to 76%. This trend is confirmed in simulations which show that not only the thickness of the ring is smaller, but also the actual number of bonds becomes smaller at larger concentrations of ligands. More specifically, the thickness of the ring drops by a factor about 3 over the entire range of ligand surface coverage.

The reason for the density dependency lies in the dynamics of ring formation. For high ligand densities, the ring closes faster than for low ligand densities. Consequently, the number of receptors diffusing into the contact zone, before crowding, is smaller for the high ligand densities than for low ligand densities allowing only for a thin ring and therefore a smaller number of bonds.

5.2. Enrichment factor

In simulations, we find that the final number of bonds is almost equal to the initial receptor density ρ_r^0 (see Fig. 8B), and only at low receptor concentrations, it is affected by the initial ligand density ρ_l^0 (see Fig. 8B inset). Such a trend emerges because the receptor density shows only little enrichment of the initial receptor density in the contact zone. This is due to the fact that at large receptor densities, bonds form over the entire contact zone which prevents further accumulation of binders. The significantly smaller ligands, in contrast, diffuse through a bond domain restoring the ligand density in the contact zone at every stage of domain formation, until the growth process is stopped by the lack of receptors.

This result agrees well with experimental observations of the enrichment factor at low temperatures (small diffusion constants). However, at high temperatures (fast diffusion) very high enrichment factors (see Fig. 9), maximizing the packing of neutravidin in the contact zone (blue doted line) are observed, even at low initial receptor densities. It was previously argued [26], that such high enrichments occur because the accumulation of receptors takes place during the spreading of the vesicle, and not after the contact zone is formed.

To confirm this hypothesis, we perform a set of simulations where the vesicle falls onto the substrate with a constant velocity v_s, i.e. the contact area changes linearly in time. Moreover, in these simulations the nucleation time is fast.

In such a scenario, the bonds start to form in a very small contact zone, and the binders accumulate in the contact zone while it is spreading. As a result, the enrichment factor becomes a function of the velocity v_s (in units of μm/s). To compare different initial ligand and receptor

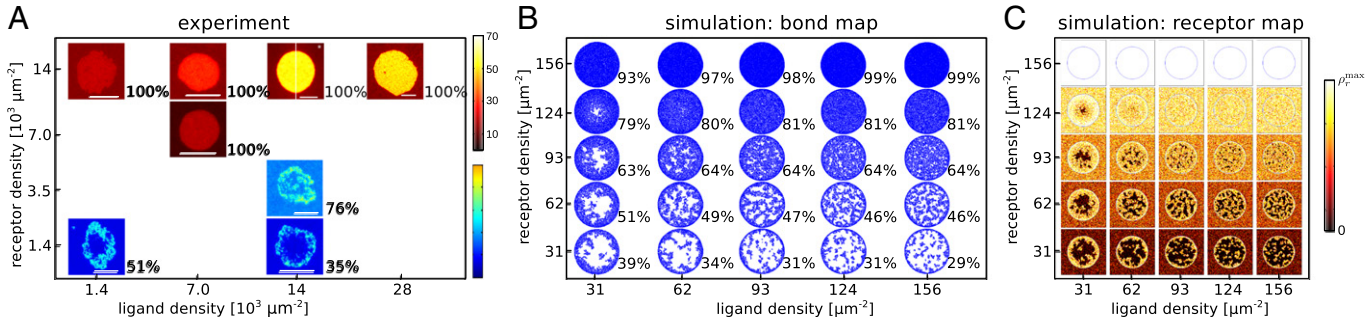

Fig. 7. Comparison of the measured (A) and simulated phase diagrams (B, C). Epifluorescent images of neutravidins in the steady state as a function of ligand and receptor coverage is shown in A. The increase in bulk concentration of receptors is seen by the change of color outside of the contact zone. The number indicates the fraction of the contact zone occupied by adhesions. The scale bar shows 10 μm and the color code in units of 10^3 μm. (B) Contact zones in the steady state obtained from simulations as a function of ligand and receptor bulk density. Bonds are marked with blue, and the respective receptors distributions are shown in (C).

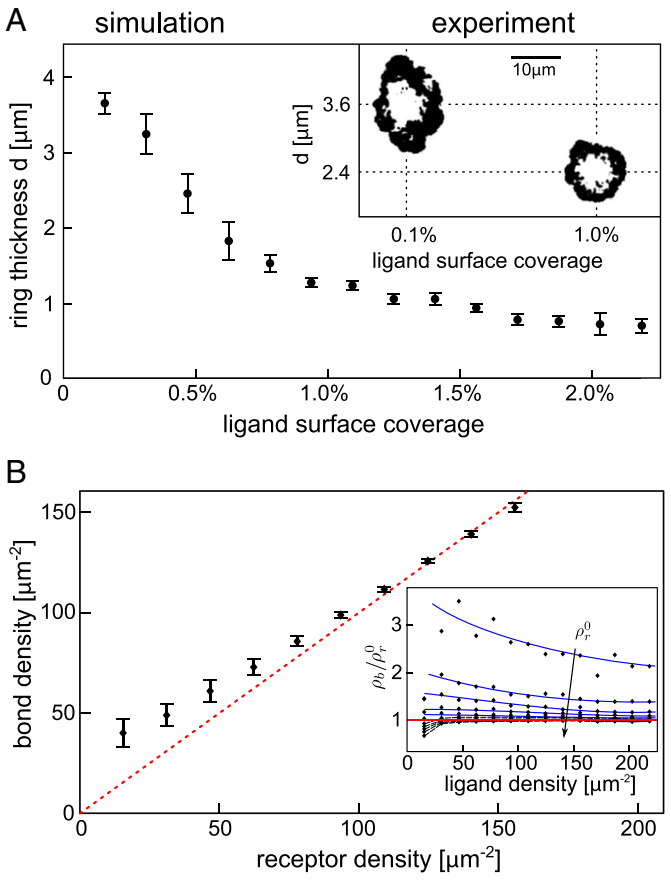

Fig. 8. (A) Ring thickness as a function of the ligand density for the simulation and the experiment (inset). Error bars mark the standard deviation for various receptor densities. Inset: Snapshots of the bond domain from the experiment (black area) for two different ligand densities. (B) Accumulated bond density ρ_b in the contact zone as a function of the initial receptor density ρ_r^0. The inset shows the normalized bond density ρ_b/ρ_r^0 as a function of the initial ligand density ρ_l^0.

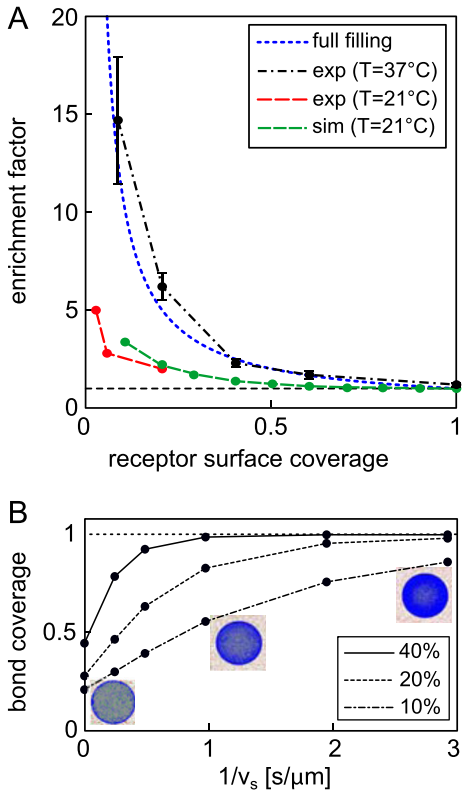

Fig. 9. (A) Enrichment factor observed experimentally at different temperatures and in simulations. The experiments presented in this work are performed at $T = 21$ °C. The enrichment factors at high temperature ($T = 37$ °C) was taken from Fenz et al. [26] (B) Simulated steady state bond coverages for vesicles spreading as the bonds are being formed. The vesicles sediment to the substrate with constant velocity v_s ($\rho_l^0 = \rho_r^0$, indicated in the legend).

densities, we show in Fig. 9 (bottom) the bond coverage in steady state. We find that as the inverse of v_s increases the thickness of the ring of crowded receptors also increases up to full packing above a critical value.

The actual value of the critical velocity depends sensitively on the concentration of both, receptors and ligands. At low ligand and high receptors densities, the reservoir of ligands may be fully depleted before the spreading is completed which results in densely packed domains in the center of the contact zone and the edge free of bonds.

6. Discussion and conclusions

In this work, we studied the interplay between the capacity of binders to diffuse through growing structures in the membrane and the morphology of these structures. We find that the initial density of bulky binders plays a major role as a control parameter for the final organization of adhesions. Furthermore, a rich phase space of growth patterns was identified, showing very similar features in simulations and experiments.

Particularly interesting are spontaneously forming ring-like structures, which arise due to the recruitment of binders into the contact zone of two membranes. If the ring is created as a consequence of accumulation of small binders (ligands), the ring structure is transient. On the other hand, if it is caused by crowding of bulky binders (receptors), the ring becomes significantly more stable, due to the inability of the large proteins to diffuse through the already established structure. Such a ring naturally creates a coral in the membrane, isolating the interior of the ring from the outside. In the cellular context, our results suggest that the formation of the ring may be passive, but the transport through the ring should involve active mechanisms. The latter seems to be the case for the T cell receptors that are transported, by coupling to the actin retrograde flow [4].

The formation of rings may be preceded by a formation of numerous small domains within the entire contact zone. This result is in agreement with recent observations of the formation of cadherin rings in the contact zone between two epithelial cells [6], where in the initial stage, multiple nucleation is promoted by homogeneous fluctuations of the composite cell membrane. However, a ring forms within a minute, at the edge of the contact zone by nucleations of small adhesions, which grow both by accumulation of cadherin from the bulk, as well as from cadherins within the emergent coral. The closure of the ring seems to provide a signal to the actin–myosin apparatus to actively exert contractile forces on the cadherin junctions, expanding the ring and increasing the contact zone. This scenario of ring-closure agrees very well with the simulations presented in this study (Fig. 7), suggesting that the initial stage of the cell–cell recognition process may rely on cadherin binding, regulated by their density and the physical properties of the cell envelope. Furthermore, our results suggest that active actin driven cell spreading couples to the development of adhesion in a highly regulated fashion, an idea which could be explored beyond the current manuscript.

Another interesting observation is the increase of the enrichment factor with the speed of the spreading of the contact zone. While this effect was demonstrated on a relatively large scale, the mechanism applies also for small contact areas. This would allow cells to regulate the density of binders in the forming of adhesions by controlling the speed of protruding lamellipodia and filopodia from the cell surface.

In conclusion, we established a Monte Carlo scheme with which we are able to understand the details of experimental observations, from the stability of bonds to the organization into macromolecular structures. Intriguingly, the micro-domain bond structures described here closely resemble those reported since more than a decade ago for integrin/TCR mediated adhesion in immune cells [1–3,5], as well as more recent reports on cadherin mediated adhesion in epithelial carcinoma cells [6]. The insights gained from the dual simulation and experimental model system can potentially identify regulating mechanisms, that can then be tested in a cellular system. Receptor crowding, arising from steric hindrance or lateral interactions, as well as ring closure, which itself is determined by molecular concentrations, interactions, and transport, have been identified here as potential important players in cell adhesion.

Acknowledgments

We thank Michael Dustin and Virgile Viasnoff for insightful discussions. A.S.S., D.S., and T.B. received funding from the European Research Council (starting grant 2013-337283), Research Training Group 1962 at Friedrich-Alexander-Universität Erlangen–Nürnberg and were supported by the Excellence Cluster: Engineering of Advanced Materials at Friedrich-Alexander-Universität Erlangen–Nürnberg. K.S. received funding from the European Research Council (307104FP/2007–2013/ERC).

Appendix A. Supplementary data

Supplementary data to this article can be found online at http://dx.doi.org/10.1016/j.bbamcr.2015.05.025.

References

[1] C. Monks, B. Freiberg, H. Kupfer, N. Sciaky, A. Kupfer, Nature 395 (1998) 82–86.
[2] A. Grakoui, S.K. Bromley, C. Sumen, M.M. Davis, A.S. Shaw, P.M. Allen, M.L. Dustin, Science 285 (1999) 221–227.
[3] Y. Kaizuka, A.D. Douglass, R. Varma, M.L. Dustin, R.D. Vale, Proc. Natl. Acad. Sci. U. S. A. 104 (2007) 20296–20301.
[4] M.L. Dustin, J.T. Groves, Annu. Rev. Biophys. 41 (2012) 543–556.
[5] P. Dillard, R. Varma, K. Sengupta, L. Limozin, Biophys. J. 107 (2014) 2629–2638.
[6] W. Engl, B. Arasi, L.L. Yap, J.P. Thiery, V. Viasnoff, Nat. Cell Biol. 16 (2014) 584–591.
[7] P.K. Tsourkas, N. Baumgarth, S.I. Simon, S. Raychaudhuri, Biophys. J. 92 (2007) 4196–4208.
[8] P.K. Tsourkas, M.L. Longo, S. Raychaudhuri, Biophys. J. 95 (2008) 1118–1125.
[9] P.K. Tsourkas, S. Raychaudhuri, Cell. Mol. Bioeng. 3 (2010) 256–268.
[10] S.Y. Qi, J.T. Groves, A.K. Chakraborty, Proc. Natl. Acad. Sci. U. S. A. 98 (2001) 6548–6553.
[11] N.J. Burroughs, C. Wülfing, Biophys. J. 83 (2002) 1784–1796.
[12] T.R. Weikl, J.T. Groves, R. Lipowsky, EPL (Europhysics Letters) 59 (2002) 916.
[13] T.R. Weikl, R. Lipowsky, Biophys. J. 87 (2004) 3665–3678.
[14] D. Coombs, M. Dembo, C. Wofsy, B. Goldstein, Biophys. J. 86 (2004) 1408–1423.
[15] H. Krobath, B. Rozycki, R. Lipowsky, T.R. Weikl, PLoS One 6 (2011) e23284.
[16] J. Brzostek, J.-G. Chai, F. Gebhardt, D.H. Busch, R. Zhao, P.A. van der Merwe, K.G. Gould, Eur. J. Immunol. 40 (2010) 2050–2059.
[17] O. Milstein, S.-Y. Tseng, T. Starr, J. Llodra, A. Nans, M. Liu, M.K. Wild, P.A. van der Merwe, D.L. Stokes, Y. Reisner, M.L. Dustin, J. Biol. Chem. 283 (2008) 34414–34422.
[18] A.-S. Smith, E. Sackmann, ChemPhysChem 10 (2009) 66–78.
[19] S.F. Fenz, K. Sengupta, Integr. Biol. 4 (2012) 982–995.
[20] E. Sackmann, A.-S. Smith, Soft Matter 10 (2014) 1644–1659.
[21] P. Streicher, P. Nassoy, M. Barmann, A. Dif, V. Marchi-Artznerm, F. Brochard-Wyart, J. Spatz, P. Bassereau, Biochim. Biophys. Acta Biomembr. 1788 (2009) 2291–2300.
[22] S.F. Fenz, A.-S. Smith, R. Merkel, K. Sengupta, Soft Matter 7 (2011) 952–962.
[23] G.I. Bell, M. Dembo, P. Bongrand, Biophys. J. 45 (1984) 1051.
[24] A.-S. Smith, U. Seifert, Soft Matter 3 (2007) 275–289.
[25] D. Schmidt, T. Bihr, U. Seifert, A.-S. Smith, EPL (Europhysics Letters) 99 (2012) 38003.
[26] S.F. Fenz, R. Merkel, K. Sengupta, Langmuir 25 (2009) 1074–1085.
[27] L. Limozin, K. Sengupta, ChemPhysChem 10 (2009) 2752–2768.
[28] A.-S. Smith, S.F. Fenz, K. Sengupta, EPL (Europhysics Letters) 89 (2010) 28003.
[29] T. Bihr, U. Seifert, A.-S. Smith, arXiv arXiv:1503.017182015.
[30] T. Bihr, U. Seifert, A.-S. Smith, Phys. Rev. Lett. 109 (2012) 258101.
[31] J. Hu, R. Lipowsky, T.R. Weikl, Proc. Natl. Acad. Sci. U. S. A. 110 (2013) 15283–15288.
[32] A.-S. Smith, K. Sengupta, S. Goennenwein, U. Seifert, E. Sackmann, Proc. Natl. Acad. Sci. U. S. A. 105 (2008) 6906–6911.
[33] E. Evans, W. Rawicz, Phys. Rev. Lett. 64 (1990) 2094–2097.
[34] S.F. Fenz, T. Bihr, R. Merkel, U. Seifert, K. Sengupta, A.-S. Smith, Adv. Mater. 23 (2011) 2622–2626.
[35] T. Bihr, S. F. Fenz, D. Schmidt, R. Merkel, K. Sengupta, U. Seifert and A.-S. Smith, in preparation.
[36] M. Avrami, J. Chem. Phys. 8 (1940) 212–224.
[37] P.L. Krapivsky, S. Redner, E. Ben-Naim, A Kinetic View of Statistical Physics, Cambridge University Press, 2010.
[38] A. Boulbitch, Z. Guttenberg, E. Sackmann, Biophys. J. 81 (2001) 2743–2751.
[39] V.B. Shenoy, L.B. Freund, Proc. Natl. Acad. Sci. U. S. A. 102 (2005) 3213–3218.
[40] H. Gao, W. Shi, L.B. Freund, Proc. Natl. Acad. Sci. U. S. A. 102 (2005) 9469–9474.
[41] T. Bihr, S. Fenz, E. Sackmann, R. Merkel, U. Seifert, K. Sengupta, A.-S. Smith, Biophys. J. 107 (2014) L33–L36.
[42] W.W. Mullins, R.F. Sekerka, J. Appl. Phys. 34 (1963) 323–329.
[43] T.A. Witten, L.M. Sander, Phys. Rev. Lett. 47 (1981) 1400–1403.